Applied Energy 247 (2019) 572–581

Contents lists available at ScienceDirect

Applied Energy

journal homepage: www.elsevier.com/locate/apenergy

Trade-off designs of power-to-methane systems via solid-oxide electrolyzer and the application to biogas upgrading

Guillaume Jeanmonod[a,1], Ligang Wang[a,b,*,1], Stefan Diethelm[a], François Maréchal[b], Jan Van herle[a]

[a] Group of Energy Materials, Swiss Federal Institute of Technology in Lausanne (EPFL), Sion, Switzerland
[b] Industrial Process and Energy Systems Engineering, Swiss Federal Institute of Technology in Lausanne (EPFL), Sion, Switzerland

HIGHLIGHTS

- Conceptual design of power-to-methane with air or oxygen sweep for biogas upgrading.
- Oxygen sweep by anode recirculation only marginally affects the system performance.
- Most biogas-upgrading systems behave similarly to the standalone power-to-methane.
- Internal methanation only beneficial at low voltage and high reactant utilization.
- Adverse effect of internal methane reforming reduced by high utilization and pressure.

ARTICLE INFO

Keywords:
Biogas upgrading
Energy storage
Power-to-methane
Solid-oxide electrolysis
Co-electrolysis
Internal methanation

ABSTRACT

Solid-oxide electrolyzer based power-to-methane is promising for large-scale energy storage as well as biogas upgrading by efficiently converting intermittent renewable power and CO_2 (e.g., in biogas) into synthetic methane. Either air or pure oxygen can be employed in solid oxide electrolyzers for anode sweeping and thermal management. This work investigates the optimal conceptual design of a variety of power-to-methane layouts to (i) identify the effect of sweep-gas type on system performance and (ii) compare different concepts for biogas upgrading. Bi-objective optimization is performed to understand the trade-off between system efficiency and methane production with the effects of the key design variables. The results indicate that oxygen sweep only marginally affected the system performance (6% reduction in methane production at the same system efficiency). The methanation inside the electrolyzer helped achieve a higher system efficiency (over 90%) by maintaining the electrolyzer temperature as high as possible. Unlike most biogas-upgrading systems, which behaved similarly to the standalone power-to-methane system, with an efficiency range of 70–86%, the direct-biogas-electrolysis performed within a wide efficiency range (52–88%) and a reduced methane yield (50% less than the other systems operating at 70% efficiency). The detrimental methane reforming inside the electrolyzer was limited by increasing the reactant conversion and the electrolysis pressure. The various solid-oxide electrolyzer based power-to-methane concepts showed promising results for biogas upgrading applications. The practical choice of biogas-upgrading concepts will depend on the requirement of operational flexibility to handle variable renewable power considering different gas storage and carbon capture technologies.

1. Introduction

The intermittency of renewable energies is a major hurdle that must be crossed to increase the penetration of renewable power [1]. To deal with the instability of renewable power and balance the electrical grid, excess renewable energy must be stored and redistributed to match the demand at different time scales [2–4]. Fast and short-term balancing of the electrical grid on the order of seconds to minutes, can be achieved using super-capacitors and flywheels; for medium-term balancing at the scale of minutes to hours batteries (e.g., flow batteries and Li-ion batteries [5]) are the major available technology; Balancing at the scale of a day to a few weeks depends highly on pumped hydro power plants

* Corresponding author at: Group of Energy Materials, Swiss Federal Institute of Technology in Lausanne (EPFL), Sion, Switzerland.
E-mail addresses: lgwangeao@163.com, ligang.wang@epfl.ch (L. Wang).
[1] These authors contributed equally to this work.

https://doi.org/10.1016/j.apenergy.2019.04.055
Received 27 January 2019; Received in revised form 8 April 2019; Accepted 14 April 2019
Available online 20 April 2019

[6–8], which are limited by geographic locations [9]. No mature technology has yet been developed to store electricity for several months at the TW h scale [7,10]. However, the concept of power-to-X, which converts renewable power to various gases (power-to-gas [11,12], e.g., H_2, CH_4 and syngas) or liquids (power-to-liquid, e.g., methanol and dimethyl ether) and other chemicals (power-to-chemical, e.g., formic acid and waxes) [13], has recently gained great interest [14]. In particular, power-to-methane (PtM) facilitates large-scale storage and transport of renewable power in the form of methane by using the already existing natural gas infrastructure [15–17]. The European gas grid has been estimated to already have the capacity to store the current annual European renewable energy production (1100 TW h) [18], which indicates that the gas grid can be seen as a large chemical battery distributed over the entire continent. Furthermore, produced methane can be efficiently converted back to electricity by fuel cells [19] or used as a substitute for fossil fuels, for, e.g., the transport sector [6,20].

Power-to-methane's system performance depends highly on the performance of electrolyzer used [21]. Compared with an alkaline or a proton-exchange membrane electrolyzer, a solid oxide electrolyzer (SOE) is advantageous due to (1) a higher electrical efficiency [22] of steam electrolysis (SE) rather than liquid-water electrolysis, (2) CO_2 electrolysis to produce CO [23], (3) direct syngas production by co-electrolysis (CE) of steam and CO_2 [24], and (4) heat-integration opportunity with other industrial processes. The system-performance bottleneck of steam electrolysis is the significant amount of heat required for steam generation [25]. However, for SOE-based PtM, this heat requirement can be largely supported (up to 80% [25]) by the heat released from the exothermic methanation reaction. Furthermore, properly selecting the SOE design points, may allow for thermally self-sufficient PtM system that requires no electrical heating [21].

An SOE can be operated with or without sweep gas (air or oxygen) at the anode channel, thus producing oxygen-enriched air or pure oxygen as by-products [26]. Economically, when the produced oxygen is sold at a price comparable to the market price of cryogenic oxygen, a reduction of up to 10% of syngas cost can be achieved [27]. Prior research have performed thermo-economic analysis on SOE-based PtM systems without sweep gas [28,29]; however, the exact contribution of the oxygen income to the price of produced methane was not mentioned. Thermodynamically, using a sweep gas is preferable for thermal management of the SOE [30]. The re-circulation of anode-outlet gas can be used to maintain adequate thermal management while still producing pure oxygen. Electrochemically, experiments have demonstrated limited impacts on the SOE stack performance when replacing air-sweep by oxygen-sweep [31].

Power-to-methane also requires CO_2, which can be extracted from various sources. Non-renewable sources mainly involve the 10–20 vol.% CO_2 flue gases from conventional power plants and cement plants [32]; however, renewable sources [33], e.g., biomass (including biogas), are more attractive to produce sustainable methane [34]. The CO_2 fraction in the streams converted from biomass can vary from 8 vol.% in flue gases to about 40 vol.% in raw biogas, and even reach 100 vol.% in fermentation processes [32], which allow less energy-intensive or even the avoidance of CO_2 capture (CC) [16]. Renewable-power driven PtM can be employed to upgrade biogas to sustainable methane for the gas-grid injection [35] with or without CC [36,37]. During biogas production, pure oxygen can be used to remove the hydrogen sulfide in biogas from aerobic bio-processes [38] without diluting the biogas (as would using air) [39], thus potentially enhancing the economic performance of biogas production [40] if pure oxygen is available as a by-product, e.g., from integrated PtM systems.

Within this context, this paper addresses the following two aspects from a system perspective that are not sufficiently investigated in literature, e.g., [41,42]:

– comparative evaluation of the effect of the anode sweep or re-circulation loop on the system performance of the SOE based PtM systems with both steam electrolysis (SE) and co-electrolysis (CE),
– comparative evaluation of the effects of different configurations (with or without CO_2 capture, SE or CE) of biogas upgrading with SOE-based PtM on the system performance.

As such, multi-objective optimization with heat cascade calculation is performed for each process concept proposed to determine the optimal trade-off designs with respect to the overall system efficiency and methane yield with the insights on the effects of design variables. The remainder of the paper is organized as follows: the investigated system concepts are presented in Section 2 with the corresponding models of the key components described in section 3. The optimization procedure used to identify the trade-off is then presented in Section 4 to obtain the results, which are presented and discussed in section 5. Finally, the conclusions are drawn in Section 6.

2. System concept

2.1. Power-to-methane with air and oxygen sweep

The SOE can be swept by air or pure oxygen, with the layout given in Fig. 1. Both systems comprise an SOE, a methanator, a membrane module for methane upgrading, a heat exchanger network, blowers and compressors. In the SE case, the SOE produces only hydrogen and CO_2 is added before entering the methanator; in the CE case, CO_2 is mixed with steam and fed into the SOE, which produces methanation-suitable syngas. The process starts with the evaporation of de-mineralized water that is then mixed with the recirculated product from the SOE outlet to guarantee a reducing atmosphere with 10 vol.% H_2, which is necessary to avoid the re-oxidation of the nickel contained in the hydrogen electrode. This mixture, i.e., the reactant feed, is further heated up to the desired temperature by the SOE outlet gases and additional electrical heating (if necessary). The reactant feed is partially reduced to H_2 (and CO when CE) in the SOE. It is then cooled down and the majority of the remaining water is separated in a flash drum. The gas mixture is then fed into the methanator integrated with an internal evaporator. The mixture out of the methanator is then cooled down with water extraction before entering the membrane separation module, from which most of the unreacted gases are sent back to the methanator.

The only difference between the air and oxygen sweep cases is the presence of the recirculating loop at the air side of the SOE. In the air-sweep case, the oxygen produced at the anode is evacuated by an air flow. In the oxygen-sweep case, the anode flow of pure oxygen is recirculated and only used for thermal management. An over-pressure valve is used to regulate the pressure and evacuate the oxygen surplus originating from the oxygen generation at the anode side. The heat available in the oxygen flow exiting the recirculating loop is utilized within the system through the heat exchanger network.

2.2. Biogas upgrading via power-to-methane

For sustainable biogas upgrading with SOE-based PtM, dynamic production of both biogas and renewable power has to be addressed with corresponding buffer storage considering the slow response (load variation) of the upgrading module. Considering the technology readiness, capacity, and specific cost of each gas storage, it may be more feasible to store intermediate gases (e.g., H_2, CO_2 or even syngas). The sizing of the upgrading module and the required storage for a given biogas site depends on the circumstance of the related renewable power production, and thus cannot be discussed in a general sense. Fortunately, the thermodynamic performances of the biogas upgrading unit are independent of the gas storage and power supply. Therefore, only the steady-state performance was evaluated to obtain an early understanding of biogas upgrading via SOE-based PtM.

The four concepts for biogas upgrading with SOE-based PtM studied

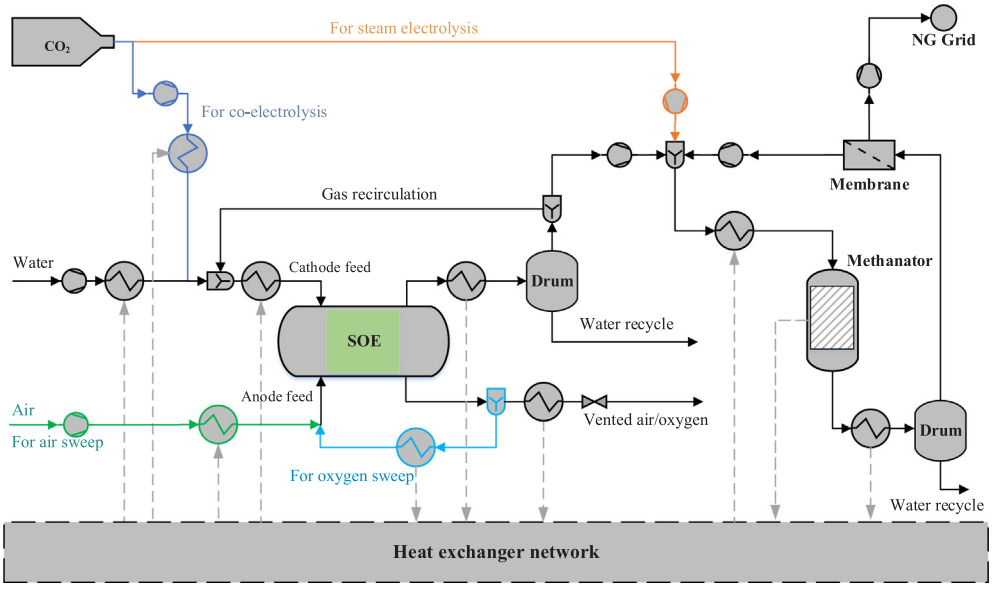

Fig. 1. Flowsheet of SOE-based power-to-methane with air sweep or oxygen recirculating loop.

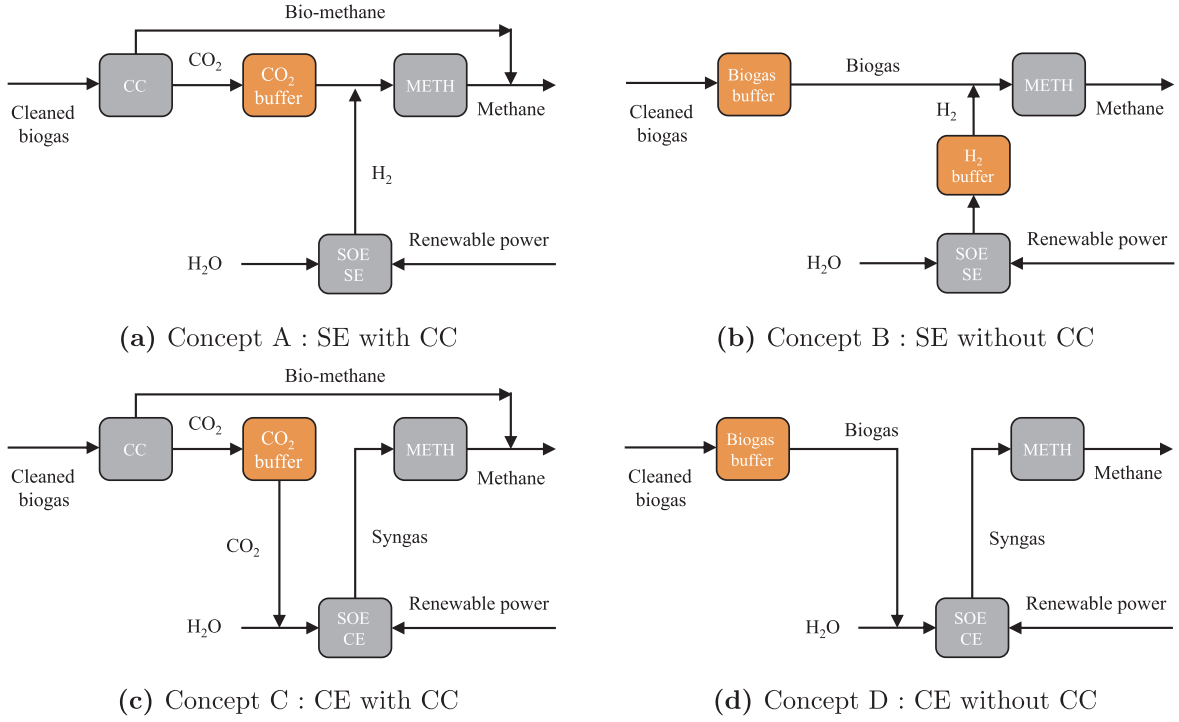

Fig. 2. System concepts of biogas upgrading via SOE-based PtM.

here are illustrated in Fig. 2. These concepts are different in the mode of electrolysis (SE/CE) and chemicals to be stored (CO_2, H_2 or biogas): (A) SE with CC and with CO_2 buffer storage, (B) SE without CC but with H_2 buffer storage, (C) CE with CC and with CO_2 buffer storage, and (D) CE without CC but with biogas buffer storage.

Many carbon capture technologies are available for biogas upgrading, including water/organic physical/amine scrubbing, pressure swing adsorption and membrane technology. A comparison of these technologies in [43,44] shows that membrane technologies are advantageous in both investment cost (due to the usually small scales of biogas production sites) and operating cost (due to reasonably low power and maintenance services required). The major disadvantage of membrane separation, i.e., low methane recovery (80–97%), can be overcome by combining with a PtM system, which recovers the remaining methane in the CO_2 stream. Membrane technology shows the best cost competitiveness for medium-scale biogas plants ($1000\,Nm^3\,h^{-1}$ bio-methane). Therefore, membrane technology was employed as the carbon capture unit for the system investigated in this paper.

The system schematic for the SOE-based biogas upgrading is illustrated in Fig. 3. The clean biogas is first heated and sent through a catalytic reactor to remove the contained O_2. Then, the biogas is further dried in a flash drum. Afterward, in concepts A and C, a two-stage membrane configuration for CO_2 capture is employed to ensure high methane purity and recovery; in concepts B and D, the biogas is sent to the PtM directly, as defined in Section 2.1 and represented in Fig. 1. For clarity, only the air sweep case is presented in Fig. 3, but a pure O_2 sweep is also possible.

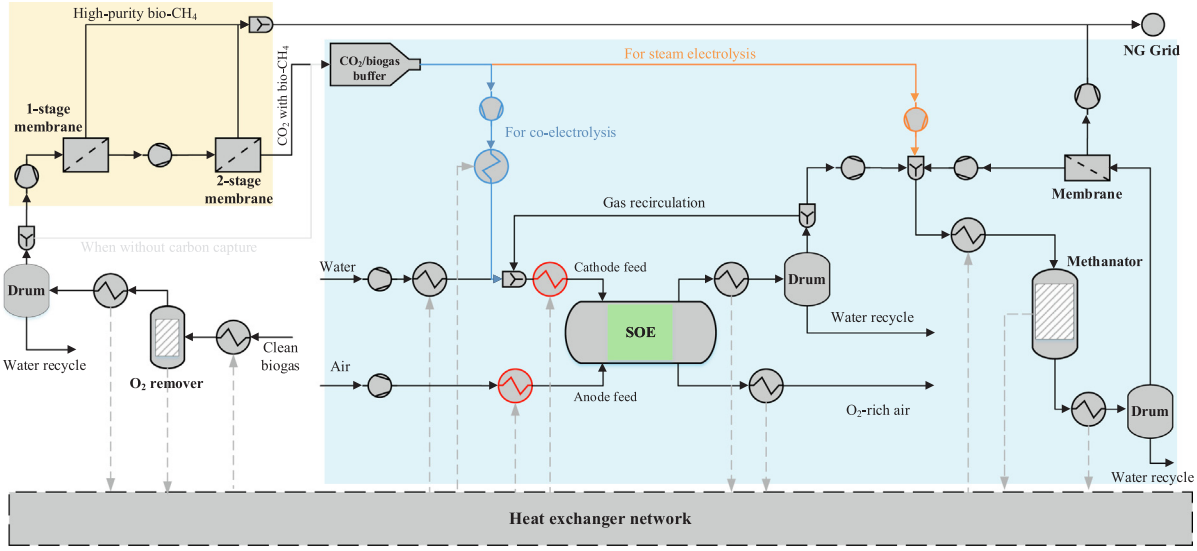

Fig. 3. System schematic for biogas upgrading via SOE-based PtM with the CC in the yellow block and PtM in the blue block (extended from [21]). The schematic can be adapted to establish the four concepts mentioned above. (For interpretation of the references to colour in this figure legend, the reader is referred to the web version of this article.)

3. Process modeling

The key components of the systems to be modeled are the SOE, the methanator, and the membrane module, each of which has been described in detail in [21]. The employed models, considerations, and specifications are briefly summarized below.

- **SOE**: A quasi-2D model, considering electro-chemistry, mass diffusion, heat transfer, and reaction kinetics that has been improved from our previous work [21] by including chemical equilibrium in the gas channel of the cathode. The improved SOE model was calibrated with the results from various experiments performed under different conditions (temperature, pressure, and gas compositions) of SE or CE at both cell and stack levels. The key parameters for both cell and stack performances were estimated to achieve good agreement between the simulation and experimental results [21]. The resulting SOE model can predict with good accuracy the electrolysis performance within wide ranges of operating variables.
- **Methanator**: An iso-thermal reactor with an inlet temperature of 240 °C and a fixed operating temperature of 290 °C was employed. The methanator was integrated with an internal steam generator to effectively extract the methanation heat, thus improving the single-pass conversion.
- **Polyimide membrane module**: A 1D model with different options of flow directions, e.g., co-flow, counter-flow or cross-flow was used. A polyimide membrane was selected for the membrane separation module because of its high selectivity and permeability of CH_4 over H_2 and CO_2 [44].
- **Heat exchanger network**: Vertical heat exchange based on the composite curve (as described in [45]) was employed to estimate the performance of the heat exchanger network. The minimum temperature differences were 10 °C for liquid streams, 20 °C for low-temperature gas streams, and 30 °C for high-temperature gas streams.
- **Remaining components**: A multi-stage gas compressor, flash drum, O_2 remover, are modeled in classical ways of chemical engineering.

4. Optimization procedure for identifying trade-off designs

A well-developed process simulation and optimization platform, as described in [21,46], was employed to investigate the impacts of operating/design variables on the system performances. The platform can readily couple various professional simulators (e.g., Aspen Plus and gPROMS) to address complex processes, allows flowsheet decomposition/reuse and easy extension of technology (flowsheet) libraries, handles mathematically-formulated heat cascade calculation and optimal utility selection, and couples evolutionary algorithms to optimize individual nonlinear processes with respect to multiple objectives [46].

Two objective functions are considered in this work: the maximization of the methane yield in normal liters per second (NL s^{-1}) from the power-to-methane process with an SOE stack of 5120 cm^2 active area, and the maximization of the system efficiency. The system efficiency was defined as follows:

$$\eta_{HHV} = \frac{\dot{E}^{HHV}_{CH_4,PtM}}{\dot{E}_{tot}}, \quad (1)$$

where $\dot{E}^{HHV}_{CH_4,PtM}$ is the energy (HHV, kW) stored in the methane produced by the PtM process, and $\dot{E}_{tot}$ is the total power (kW) consumed by the entire system (including the SOE and all of the auxiliaries).

The design variables considered and their bounds are listed in Table 1. The SOE inlet temperature was fixed at 700 °C for all cases to give the basis of performance comparison. Within these bounds, the SOE can operate with sweep air or pure O_2. Defining reactant utilization is not easy for CE, especially when internal methanation is involved, as the steam is simultaneously electro-chemically converted to hydrogen and oxygen, and catalytically consumed or produced by the water-gas shift and methanation reactions. Therefore, an apparent utilization factor considering only the share of electro-chemical conversion was employed and defined as follows:

$$U_F = \frac{I}{n\dot{N}_R\mathcal{F}}, \quad (2)$$

where U_F is the electro-chemical utilization factor, I the total current in A, n is the number of electrons exchanged during the electro-chemical processes (i.e., $n = 2$ for H_2O and CO_2 reduction), $\dot{N}_R$ is the molar flow of reactant (only H_2O and CO_2) in mol s^{-1}, and $\mathcal{F}$ is the Faraday constant (96,485 C mol^{-1}). For membrane-based separation, the area of each module was not specified but determined by the specified target of the methane purity (i.e., 96 vol.%). Given the inlet temperature, pressure, utilization factor and steam/sweep feed flow rates, the operating current density, voltage and outlet temperature of the SOE were determined iteratively. If the outlet temperature of a solution was over

Table 1
Decision variables[a] and bounds.

Variable	Bounds	Variable	Ranges
SOE pressure	1–30 bar	METH reactor pressure	2–30 bar
SOE utilization factor[b]	30–80%	METH permeate pressure	0.5–10 bar
SOE steam feed flow rate	0.5–15 sccm cm^{-2}	CC feed pressure	6–10 bar
SOE sweep air flow rate[c]	0.1–40 sccm cm^{-2}	CC permeate pressure	0.5–3 bar

[a] The SOE inlet temperature is fixed at 700 °C with a maximum allowed temperature difference inside the stack of 120 °C (derived from practical applications).
[b] The utilization factor is defined as the share of inlet reactants (H_2O and/or CO_2) converted electro-chemically, which is also referred to as electro-chemical utilization factor.
[c] When sweep-air flow rate is set as 0.1 sccm cm^{-2}, the SOE is operated under pure O_2 production.

820 °C or below 580 °C (rarely the case), indicated a temperature difference inside the stack of over 120 °C, a penalty was assigned to discard this solution during the optimization run. After the multi-objective optimization, a set of Pareto-optimal solutions were obtained, which revealed the trade-off between the two considered objective functions. With the Pareto front, the impacts of the listed decision variables on the objective functions can be identified to assist the selection of operating/design variables.

5. Results and discussions

It was shown [21] that, for a given SOE hardware, the system efficiency decreases as the methane yield increases (current density). This is mainly caused by the increase in voltage (over-potential) that occurs with an increase in current density, which results in the change of the electro-chemical performance, plant-wise heat integration, and stack cooling requirement. Detailed explanations have been discussed by [21] for the air-sweep case as defined in Fig. 1. The Pareto fronts obtained in this study follow similar trends.

5.1. The effects of oxygen sweep

Although the methane yield with respect to the system efficiency presented a similar trend for both the air- and oxygen-sweep, the oxygen-sweep cases generally showed lower performances than the air-sweep cases (6% reduction of methane yield), as shown in Fig. 4. For the SE, oxygen sweep slightly lowered the methane yield when system efficiency was below 80%; above that efficiency, the methane yields for both air- and oxygen-sweep cases were almost equal. For CE, the methane production using oxygen sweep was slightly lower until 87% efficiency, above which the methane yield was enhanced to the same level as the air-sweep cases. The sweep type (whether air or oxygen) had only a limited impact on the electrolysis performance at system efficiencies and almost no impact at higher efficiencies. Therefore, practically, the selection of sweep type depends on the economic

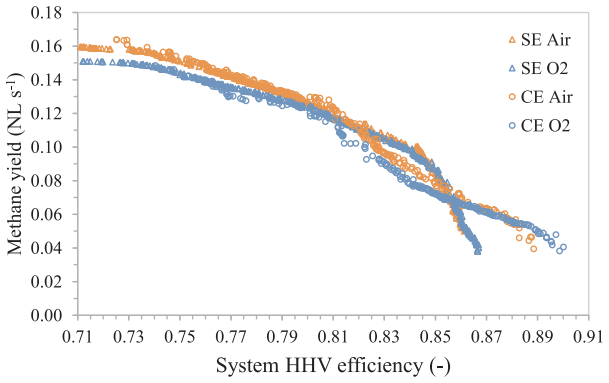

Fig. 4. Methane yield with respect to the system efficiency for SE and CE cases with air and oxygen sweep.

assessment by considering (1) the additional income related to the sale of the oxygen produced and (2) the potential extra cost related to the handling of pure oxygen especially at high temperature (i.e., highly oxidant atmosphere). A detailed analysis of the corresponding variations of design variables for both the SE and CE cases is presented in the next sections.

5.1.1. Insight on the steam-electrolysis cases

The evolution of selected operating parameters with respect to the system efficiency is presented in Fig. 5. Despite similar Pareto fronts (Fig. 4), the air- and oxygen-sweep cases had different optimal operating conditions, especially below 85% efficiency.

For both cases presented in Figs. 5(a) and 5(b), the maximum methane yield corresponds to the lowest efficiency and the highest sweep feed. A high methane yield requires a high current density, which results in a high operating voltage and thus more heat released in the stack to be extracted by an increased sweep gas. The oxygen sweep flow rate was consistently higher than the air-sweep case, excepted when the efficiency dropped below 75%. In this region, the air-sweep case employed the maximum sweep-gas flow rate considered, whereas the flow rate was only gently reduced with a decreasing voltage in the oxygen-sweep case. As no extra cooling can be provided in the air-sweep case, the voltage was limited to approximately 1.45 V (below the upper bound, 1.5 V). As the efficiency increased from 71% to 75% (77%) for the air- (oxygen-) sweep case, respectively, the average cell voltage decreased to a bend (Fig. 5(e) and (f)) that also corresponded to the maximum sweep flow rate considered. This marks the transition from a region where the reactant flow rate decreased more sharply than the sweep flow rate to the inverted situation. When the sweep gas could not be adjusted any more, the stack cooling relied mainly on the reactant flow. Any increase in the applied current (thus internal heat release) was addressed by an additional increase in the reactant flow (thus a decrease in reactant utilization). This emphasizes the importance of the anode sweep gas on the thermal management and performance of the SOE stack.

Below about 76% efficiency, the reactant utilization of the oxygen-sweep case was rather low (50%), resulting in high heat demand for steam generation. This increase in heat demand could be fulfilled by increasing the methanation pressure, which could (1) improve the heat-recovery potential in the stream exiting the methanator and (2) promote the methane production thus increasing the heat released per pass. In the air-sweep case, the methanation pressure slowly increased from 7 to 10 bar as the system efficiency decreased from 76 to 71% (Fig. 5(d)). In this efficiency range, the reactant conversion was higher and the reactant feed was lower for the air-sweep case, compared with the oxygen-sweep case (Fig. 5(b) and (a)). The heat demand in the air sweep case was thus lower than that in the oxygen-sweep case, and the methanator pressure did not need to be excessively increased as was necessary for the oxygen-sweep case.

The reactant conversion increased nearly linearly from 48% (38%) for the air (oxygen) sweep case, to an upper limit of 80%, which was reached at 85% efficiency in both cases (Fig. 5(a) and (b)). The reactant

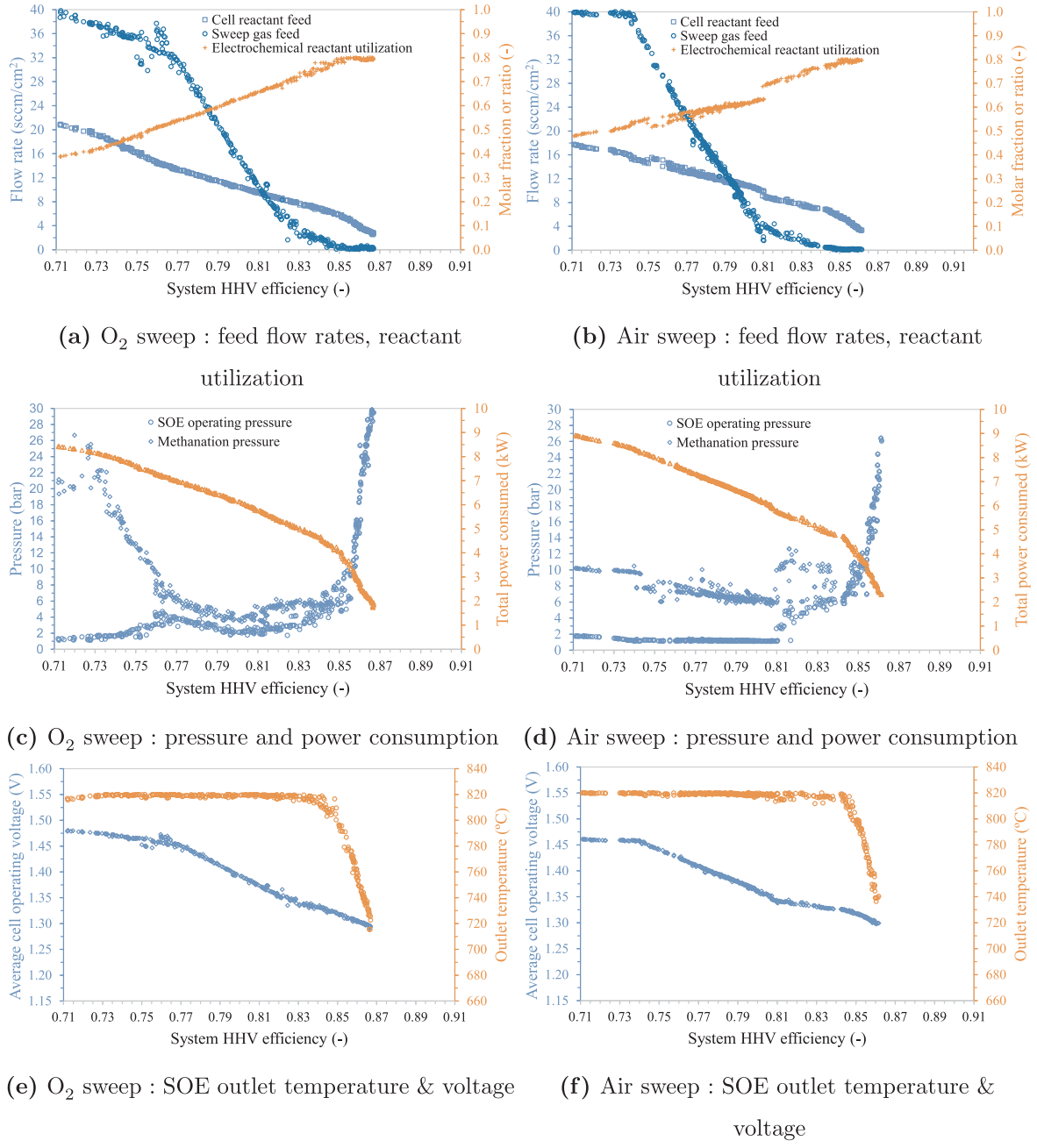

(a) O_2 sweep : feed flow rates, reactant utilization

(b) Air sweep : feed flow rates, reactant utilization

(c) O_2 sweep : pressure and power consumption

(d) Air sweep : pressure and power consumption

(e) O_2 sweep : SOE outlet temperature & voltage

(f) Air sweep : SOE outlet temperature & voltage

Fig. 5. Insights of the Pareto solutions in steam electrolysis.

conversion was lower in the oxygen-sweep case at efficiencies below 80% to counterbalance the higher concentration over-potential due to the operation with pure oxygen (Fig. 5(a)). At 80% efficiency, the methane yield and efficiency were the same for the air- and oxygen-sweep cases, although the voltage was 30 mV higher for the oxygen-sweep case. Furthermore, the total power consumed by the PtM system was equal for both the air- and oxygen-sweep cases (Fig. 5(d) and (c)). This suggests that the power consumed by the auxiliaries was smaller in the oxygen- than in the air-sweep case and compensates for the higher losses relative to higher operating voltages. In the efficiency range of 76–84%, the methanator pressure was approximately 2.6 and 7 times higher than the SOE pressure was in the oxygen- and air-sweep case, respectively. Thus the compression work for the methanator in the oxygen-sweep case was less than that of the air-sweep case. However, the air-sweep case presented a lower SOE pressure, which can be advantageous as the close-to-atmospheric-pressure SOE may become commercially available earlier than the pressurized SOE. The methanator pressure can be as low as below 6 bar for both the air- and oxygen- sweep cases.

The methane production dropped drastically at efficiencies above 85% efficiency, whereas the methanator and SOE pressures were equal and increased remarkably with the increasing efficiency (Figs. 4, 5(c) and (d)). The SOE pressure was increased to improve the mass diffusion, which became critical to reach high reactant conversion at a low reactant-feed flow rate. Consequently, the methanation pressure was elevated to remain above the electrolysis pressure, thus avoiding throttling or additional expansion. A large drop of the SOE outlet temperature was also observed (Fig. 5(e) and (f)), due to the decrease of internally generated heat in the stack with decreased voltage and thus improved electrochemical performance (Fig. 5(e) and (f)). Therefore, no sweep gas was needed for additional stack cooling (Fig. 5(a) and (b)). In this region, the system performances were limited by the

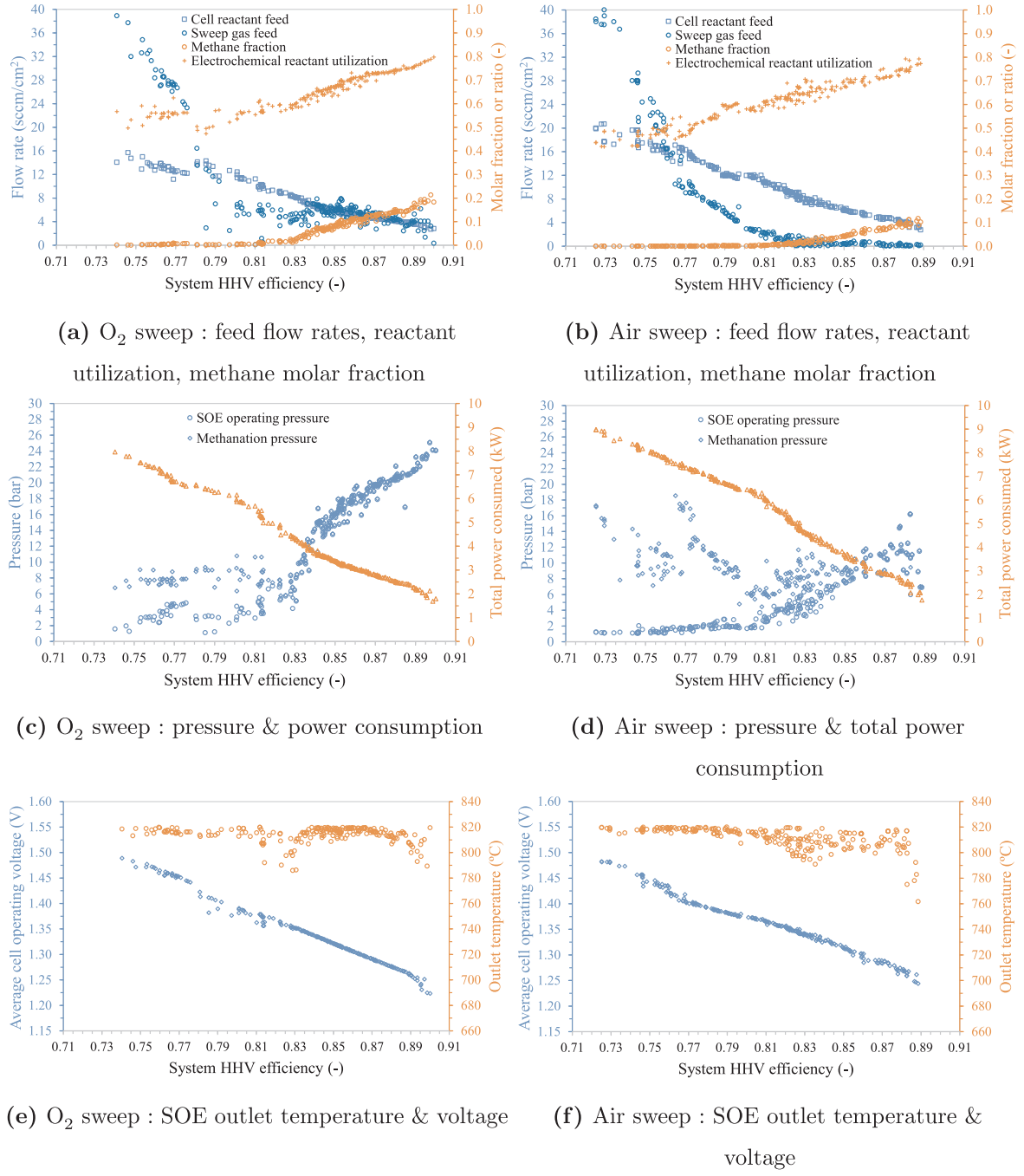

(a) O_2 sweep : feed flow rates, reactant utilization, methane molar fraction

(b) Air sweep : feed flow rates, reactant utilization, methane molar fraction

(c) O_2 sweep : pressure & power consumption

(d) Air sweep : pressure & total power consumption

(e) O_2 sweep : SOE outlet temperature & voltage

(f) Air sweep : SOE outlet temperature & voltage

Fig. 6. Insights of the Pareto solutions with co-electrolysis.

reactant conversion and operating voltage. To keep a high stack temperature at a voltage below the thermoneutral voltage, sweep gas could be used as a heat source to carry heat from other industrial processes to the stack as suggested by [30].

5.1.2. Insight on the co-electrolysis cases

Similarly to the SE cases, the Pareto fronts of the oxygen- and air-sweep cases of the CE cases were similar (Fig. 4) but showed a different evolution of the system operating conditions with respect to the system efficiency, as presented in Fig. 6.

For the designs with an efficiency below 83%, the air-sweep cases showed a higher methanator pressure and a lower SOE pressure when compared with the oxygen-sweep cases (Fig. 6(c) and (d)). The pressure ratio between the SOE and methanator for the oxygen-sweep case was lower, similar to the results obtained for the SE cases for efficiency above 76%. However, unlike the oxygen-sweep SE case (Fig. 5(c)), the methanator pressure of the oxygen-sweep CE case did not rise as the efficiency decreased (Fig. 6(c)) but rather stabilized at around 7–8 bar. This is due to the decreased heat demand for steam generation as the CO methanation reaction ($3H_2 + CO \rightarrow CH_4 + H_2O$, $\Delta_r H^0_{298} = -206\,\text{kJ mol}^{-1}$) dominates in CE cases rather than CO_2 methanation ($4H_2 + CO_2 \rightarrow CH_4 + 2H_2O$, $\Delta_r H^0_{298} = -165\,\text{kJ mol}^{-1}$), thus (1) a smaller amount of hydrogen (steam and heat) is needed for the same methane yield, and (2) CO methanation is more exothermic with more heat available to support steam generation [28].

Unlike the SE cases (Fig. 5(e) and (f)), the SOE outlet temperature did not drop when the voltage approached or dropped below the thermoneutral voltage (Fig. 6(e) and (f)). This is due to the internal

methanation promoted under pressurized conditions. Starting from the designs of around 83% efficiency, the SOE pressure became sufficiently high to generate a significant fraction of methane inside the stack (Fig. 6(c) and (d)), thus releasing sufficient heat to compensate for the heat needed by the endothermal operation. The maintained SOE temperature allowed a further decrease in the voltage, thus increasing the system efficiency above 90% (higher than the SE cases).

When internal methanation became preferred (i.e., above 83% efficiency), the outlet methane fraction in the oxygen-sweep case was higher than that of the air-sweep case at the same efficiency with a similar reactant feed (Fig. 6(a) and (b)). This is the consequence of higher SOE pressure in the oxygen-sweep case (Fig. 6(c) and (d)), which shifts the thermodynamic equilibrium towards methane formation. Internal methanation thus became a source of heat as well as steam, improving the electrochemical performance with enhanced mass diffusion, thus compensating for the increased over-potential related to the oxygen partial pressure. The oxygen-sweep CE case always required sweep gas, even at very high efficiencies (Fig. 6(a)); however, for the air-sweep case above 83% efficiency, no sweep gas was needed. This is due to the difference in the system layouts. In the air-sweep case (Fig. 1), sweep air is taken from the atmosphere and compressed to the SOE pressure, whereas in the oxygen-sweep case (Fig. 1), the sweep is re-circulated, thus requiring less compression work for the same amount of sweep gas. The extraction of excess heat from internal methanation by sweep gas can be at almost no cost in the oxygen-sweep case but is punished largely by the gas compression in the air-sweep case. Therefore, the sweep-gas re-circulation becomes particularly interesting for thermal management of the stack under pressurized operation.

5.2. Biogas upgrading via solid-oxide electrolyzer based power-to-methane

It has been concluded in the above sections that there were no substantial differences between the air- and oxygen-sweep cases. Therefore, only air-sweep was considered in this section.

The trade-offs between the methane yield and system efficiency are illustrated in Fig. 7 for all cases. The performances of the SE concepts A and B were very similar to each other, particularly before the turning points of each front, and were in line with the results of Section 2.1 and those found by [21]. Concept B performed slightly better when the system efficiency was over 83%. The CE concept C also presented similar performances than the one reported in section 2.1 but the concept D shows a quite different profile. The CE concepts C and D generated less methane at the same system efficiency, especially concept D with direct CE of biogas (50% less than the other system operating at 70% efficiency). However, concepts C and D allowed designs with much higher efficiency than those of the concepts A and B (around 4 percentage points higher). Concept D allowed system designs/operating points with a wide range of efficiency, 50–88%. When the system efficiency of concept C was below 78%, the Pareto front nearly overlapped with that of concepts A and B; however, at system efficiencies above 78%, a drop in terms of total methane (both bio-methane and synthetic methane) production occurred. As concepts A and B did not show major differences than the SE cases discussed in Section 2.1 and [21], only concepts C and D are further discussed below.

5.2.1. Insight on concepts C and D

The profiles of most decision variables in concept C with respect to the system efficiency (Fig. 8(a) and (b)) were similar to those of the air-sweep CE case (Fig. 6(b) and (d)) but were shifted to a lower efficiency due to the additional electricity consumption related to the CC. The increase in the SOE pressure was more important in the concept C than in the air-sweep CE PtM case, when a comparable efficiency range is considered, 80–86% and 83–89%, respectively. The internal methanation reaction was thus increased in the concept C, allowing the methane molar fraction to reach over 15% for the designs with the highest efficiency. The heat released from the internal methanation was absorbed by the electro-chemical reactions and prevented the drops of the SOE temperature and performance, as explained in Section 2.1.

For concept D (Fig. 8(c) and (d)) pressurized stack operation over 10 bar (Fig. 8(d)) was preferred to reduce or prevent the reforming of bio-methane inside the stack within the efficiency range 70–88%. Due to the extra cooling offered by the bio-methane fed into the stack, the designs with almost no sweep air shifted to lower efficiency. The sweep-air flow rate and the internal reforming of bio-methane, i.e., the two major stack-cooling abilities, increased with the rising voltage to avoid overheating the stack. However, the internal reforming rate of the bio-methane must be well controlled to ensure that the stack temperature remains as high as possible to achieve the best electro-chemical performance. Particularly, for a low reactant utilization, the SOE pressure should be elevated to prevent excessive bio-methane reforming. Above 73% efficiency, the cooling from sweep air was no longer needed, as the voltage dropped too low to maintain the high stack temperatures necessary to further enhance the system efficiency. Thus, internal methanation was favored at a low voltage, as presented in Section 5.1.2. Along with the increase in the system efficiency, the preferred SOE pressure was found to decrease with an increase in reactant utilization to properly control the internal methane reforming for a preferred stack temperature. Considering the internal methanation reaction ($4H_2 + CO_2 \leftrightarrow CH_4 + 2H_2O$, $\Delta_r H^0_{298} = -165\,\text{kJ mol}^{-1}$), the reaction rate can be effectively controlled by varying the partial pressures between the reactants and products by increasing (a) the reactant utilization and (b) the total pressure. Factor (a) might have more influence than the factor (b), since a high reactant utilization reduces the partial pressure of H_2O and simultaneously increases that of H_2, which can strongly enhance the driving force for CH_4 production. Therefore, as shown in Fig. 8, even a high SOE pressure was needed to avoid excessive steam reforming with a low reactant utilization, whereas a low SOE pressure can promote internal methanation with a high reactant utilization.

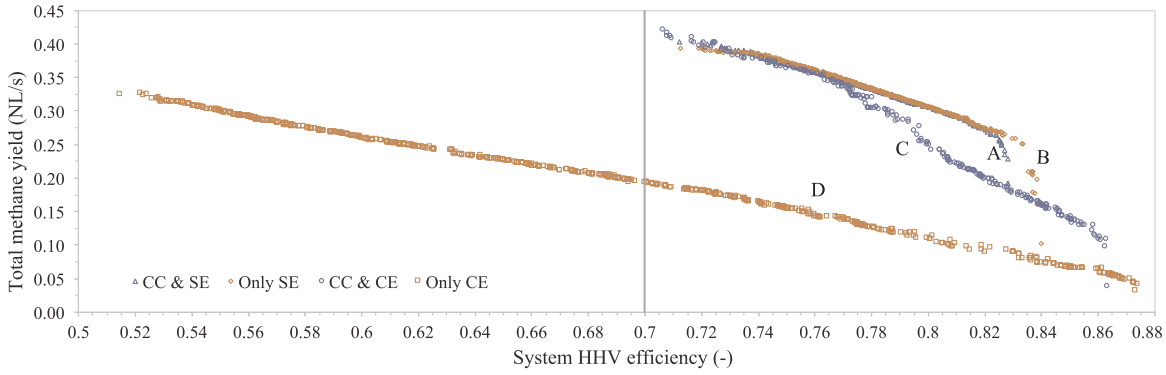

Fig. 7. Comparison of the thermodynamic performance (Pareto fronts) of the four concepts (A–CC & SE; B–only SE; C–CC & CE; D–only CE).

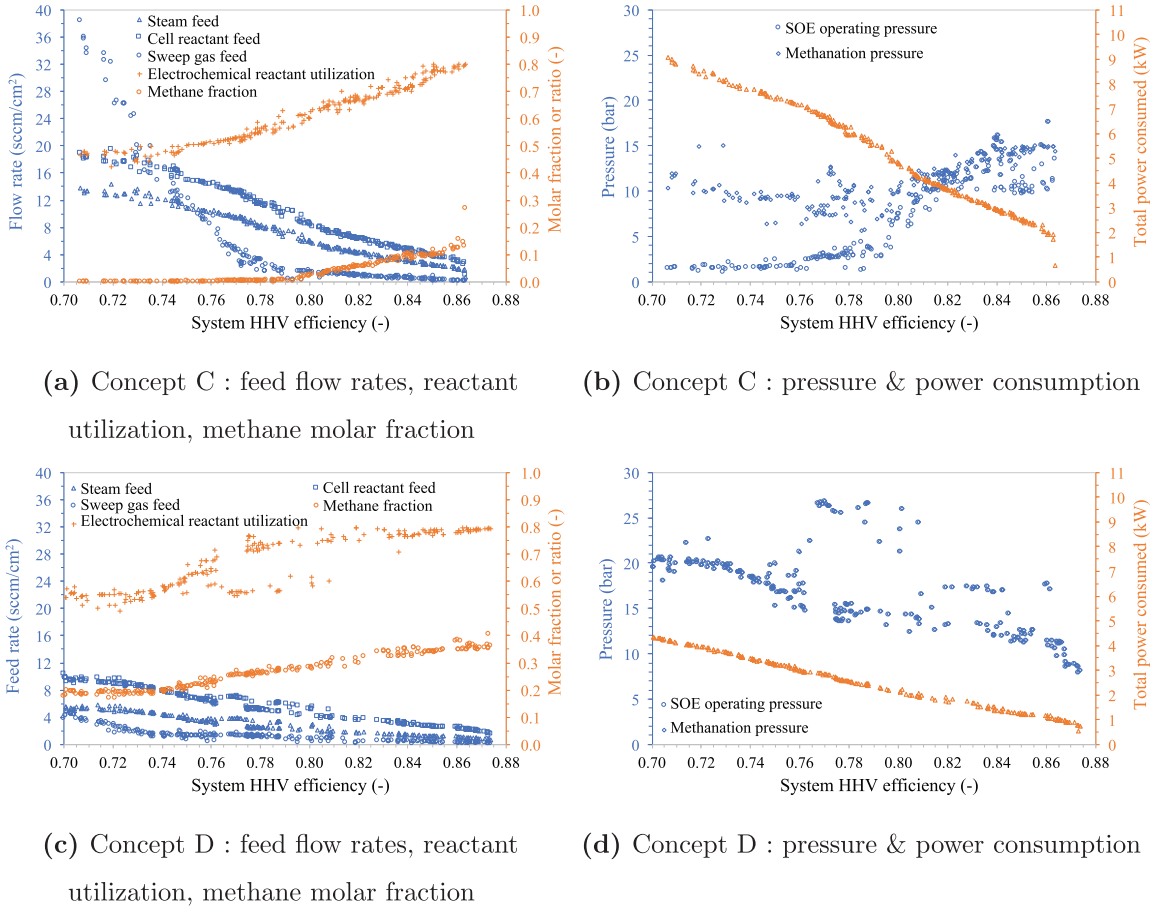

(a) Concept C : feed flow rates, reactant utilization, methane molar fraction

(b) Concept C : pressure & power consumption

(c) Concept D : feed flow rates, reactant utilization, methane molar fraction

(d) Concept D : pressure & power consumption

Fig. 8. Insights of the Pareto solutions with system efficiency over 70% for the co-electrolysis concepts.

However, the concept D likely provides the least profitable concept due to the much lower methane yield and higher operational complexity required to properly control the internal methane-steam-reforming. The concept C showed a lower methane yield than the concepts A and B between 77% and about 83%, but can reach higher efficiency and may reduce the methanator size due to internal methanation. Thus, the selection among the concepts A, B, and C, depends mainly on an economic evaluation considering the costs of the CC, methanator, and gas storage necessary to accommodate the mismatch between the biogas production and renewable power supply.

6. Conclusion

A multi-objective optimization platform and calibrated component models were used to investigate and compare the optimal design points of: (1) solid-oxide electrolyzer based power-to-methane systems considering both steam- and co-electrolysis operation with oxygen- and air-sweep and (2) four biogas-upgrading concepts via solid-oxide electrolyzer based power-to-methane covering steam- or co-electrolysis with or without carbon capture. The main conclusions include:

- Oxygen-sweep only marginally affects the methane yield of the power-to-methane system (6% reduction of methane yield for the same system efficiency). The re-circulation of the oxygen sweep could even be profitable under high electrolysis pressure, compared to the air-sweep cases, as sweep-gas re-circulation reduced the required compression work.
- Independent from sweep-gas type, a similar trade-off between system efficiency and methane yield was found for both steam- and co-electrolysis cases. The highest efficiency (90%) was reached with co-electrolysis at the cost of a reduced methane yield (only about 25% of the maximum achievable methane yield), while steam-electrolysis was preferred at a lower efficiency range (82–86%).
- To achieve a high system efficiency, high reactant utilization and stack pressure were favored with small reactant and sweep-gas feeds and low current density (voltage). Under such conditions, internal methanation provides an internal heat source to maintain high stack temperature at a low voltage and an internal steam source to enhance mass diffusion at a high reactant utilization.
- The biogas upgrading concepts in steam-electrolysis with and without carbon capture and in co-electrolysis with carbon capture behaved similarly with those of the corresponding power-to-methane systems only with maximal efficiency of 83%, 84%, and 86%, respectively, about 3 to 4 percentage points lower than those of the power-to-methane systems alone.
- The direct biogas co-electrolysis case produced less synthetic methane (50% less than the other system operating at 70% efficiency) but can reach even higher system efficiency (over 87%). The adverse effect of internal methane reforming on the system efficiency could be reduced by increasing the reactant utilization and electrolysis pressure. However, despite requiring no carbon capture and only biogas storage, direct biogas upgrading is probably the least favored concept.

Solid-oxide electrolyzer based power-to-methane system applied to biogas upgrading was shown to be promising for efficiently storing renewable energy. A thermo-economic analysis of the various concepts proposed should be performed to evaluate their economic feasibility. The focus should be set on the design/sizing of the gas storage (buffer) for maximizing the availability of the systems and on the evaluation of

the potential benefit of pure oxygen production especially within the context of biogas upgrading where oxygen can be used for desulfurization.

Acknowledgements

The research leading to the presented work is funded by European Union's Horizon 2020 under grant agreements n° 699892 (ECo) and n° 731224 (BALANCE). The study was also partially conducted in relation to the Swiss Competence Center for Energy Research (SCCER) 'BioSWEET' on Biogas valorisation paths.

References

[1] Denholm P, Hand M. Grid flexibility and storage required to achieve very high penetration of variable renewable electricity. Energy Policy 2011;39(3):1817–30. https://doi.org/10.1016/j.enpol.2011.01.019. < http://www.sciencedirect.com/science/article/pii/S0301421511000292 > .

[2] Yekini Suberu M, Wazir Mustafa M, Bashir N. Energy storage systems for renewable energy power sector integration and mitigation of intermittency. Renew Sust Energy Rev 2014;35:499–514. https://doi.org/10.1016/j.rser.2014.04.009.

[3] Zappa W, Junginger M, van den Broek M. Is a 100% renewable European power system feasible by 2050? Appl Energy 2019;233–234:1027–50. https://doi.org/10.1016/j.apenergy.2018.08.109. < http://www.sciencedirect.com/science/article/pii/S0306261918312790 > .

[4] McPherson M, Tahseen S. Deploying storage assets to facilitate variable renewable energy integration: the impacts of grid flexibility, renewable penetration, and market structure. Energy 2018;145:856–70. https://doi.org/10.1016/j.energy.2018.01.002. < http://www.sciencedirect.com/science/article/pii/S0360544218300021 > .

[5] Díaz-González F, Sumper A, Gomis-Bellmunt O, Villafáfila-Robles R. A review of energy storage technologies for wind power applications. Renew Sust Energy Rev 2012;16(4):2154–71.

[6] Aneke M, Wang M. Energy storage technologies and real life applications – a state of the art review. Appl Energy 2016;179:350–77. https://doi.org/10.1016/j.apenergy.2016.06.097. < http://www.sciencedirect.com/science/article/pii/S0306261916308728 > .

[7] Waidhas M. Business opportunities for MW electrolysis and related requirements; 2017.

[8] Palizban O, Kauhaniemi K. Energy storage systems in modern grids–matrix of technologies and applications. J Energy Storage 2016;6:248–59. https://doi.org/10.1016/j.est.2016.02.001. < http://www.sciencedirect.com/science/article/pii/S2352152X1630010X > .

[9] Yang C-J. Chapter. In: Letcher TM, editor. Storing energy 2 – pumped hydroelectric storage Oxford: Elsevier; 2016. p. 25–38. https://doi.org/10.1016/B978-0-12-803440-8.00002-6.

[10] Luo X, Wang J, Dooner M, Clarke J. Overview of current development in electrical energy storage technologies and the application potential in power system operation. Appl Energy 2015;137:511–36. https://doi.org/10.1016/j.apenergy.2014.09.081. < http://www.sciencedirect.com/science/article/pii/S0306261914010290 > .

[11] Schiebahn S, Grube T, Robinius M, Tietze V, Kumar B, Stolten D. Power to gas: technological overview, systems analysis and economic assessment for a case study in Germany. Int J Hydrogen Energy 2015;40(12):4285–94. https://doi.org/10.1016/j.ijhydene.2015.01.123. < http://www.sciencedirect.com/science/article/pii/S0360319915001913 > .

[12] Samsatli S, Samsatli NJ. The role of renewable hydrogen and inter-seasonal storage in decarbonising heat–comprehensive optimisation of future renewable energy value chains. Appl Energy 2019;233–234:854–93. https://doi.org/10.1016/j.apenergy.2018.09.159. < http://www.sciencedirect.com/science/article/pii/S0306261918314715 > .

[13] Blanco H, Faaij A. A review at the role of storage in energy systems with a focus on Power to Gas and long-term storage. Renew Sust Energy Rev 2018;81:1049–86. https://doi.org/10.1016/j.rser.2017.07.062. < http://www.sciencedirect.com/science/article/pii/S1364032117311310 > .

[14] Mennicken L, Janz A, Roth S. The German R&D program for CO2 utilization-innovations for a green economy. Environ Sci Pollut Res 2016;23(11):11386–92. https://doi.org/10.1007/s11356-016-6641-1.

[15] Thellufsen JZ, Lund H. Cross-border versus cross-sector interconnectivity in renewable energy systems. Energy 2017;124:492–501. https://doi.org/10.1016/j.energy.2017.02.112. < http://www.sciencedirect.com/science/article/pii/S0360544217302943 > .

[16] Ghaib K, Ben-Fares F-Z. Power-to-methane: a state-of-the-art review. Renew Sust Energy Rev 2018;81:433–46. https://doi.org/10.1016/j.rser.2017.08.004. < http://www.sciencedirect.com/science/article/pii/S1364032117311346 > .

[17] Uyar TS, Beşikci D. Integration of hydrogen energy systems into renewable energy systems for better design of 100% renewable energy communities. Int J Hydrogen Energy 2017;42(4):2453–6.

[18] De Buck P. Energy transition in Europe: the case for gas and gas infrastructure; 2018.

[19] Suciu R, Girardin L, Maréchal F. Energy integration of CO2 networks and power to gas for emerging energy autonomous cities in Europe. Energy 2018;157:830–42. https://doi.org/10.1016/j.energy.2018.05.083. < http://www.sciencedirect.com/science/article/pii/S0360544218309034 > .

[20] Engerer H, Horn M. Natural gas vehicles: an option for Europe. Energy Policy 2010;38(2):1017–29. https://doi.org/10.1016/j.enpol.2009.10.054. < http://www.sciencedirect.com/science/article/pii/S0301421509008131 > .

[21] Wang L, Pérez-Fortes M, Madi H, Diethelm S, herle JV, Maréchal F. Optimal design of solid-oxide electrolyzer based power-to-methane systems: a comprehensive comparison between steam electrolysis and co-electrolysis. Appl Energy 2018;211:1060–79. https://doi.org/10.1016/j.apenergy.2017.11.050.

[22] Ferrero D, Lanzini A, Santarelli M, Leone P. A comparative assessment on hydrogen production from low- and high-temperature electrolysis. Int J Hydrogen Energy 2013;38(9):3523–36. https://doi.org/10.1016/j.ijhydene.2013.01.065. < http://www.sciencedirect.com/science/article/pii/S0360319913001511 > .

[23] Kaur G, Kulkarni AP, Giddey S, Badwal SPS. Ceramic composite cathodes for CO2 conversion to CO in solid oxide electrolysis cells. Appl Energy 2018;221:131–8. https://doi.org/10.1016/j.apenergy.2018.03.176. < http://www.sciencedirect.com/science/article/pii/S0306261918305269 > .

[24] Graves C, Ebbesen SD, Mogensen M. Co-electrolysis of CO2 and H2O in solid oxide cells: performance and durability. Solid State Ion 2011;192(1):398–403.

[25] Wang L, Düll J, Maréchal F, Van herle J. Trade-off designs and comparative exergy evaluation of solid-oxide electrolyzer based power-to-methane plants. Int J Hydrogen Energy. doi:https://doi.org/10.1016/j.ijhydene.2018.11.151. < http://www.sciencedirect.com/science/article/pii/S0360319918337832 > .

[26] Liu T-L, Wang C, Hao S-J, Fu Z-Q, Peppley BA, Mao Z-M, et al. Evaluation of polarization and hydrogen production efficiency of solid oxide electrolysis stack with La0.6sr0.4co0.2fe0.8o3 Ce0.9gd0.1o1.95 oxygen electrode. Int J Hydrogen Energy 2016;41(36):15970–8. https://doi.org/10.1016/j.ijhydene.2016.04.243.

[27] Fu Q, Mabilat C, Zahid M, Brisse A, Gautier L. Syngas production via high-temperature steam/CO2 co-electrolysis: an economic assessment. Energy Environ Sci 2010;3(10):1382–97. https://doi.org/10.1039/C0EE00092B. < https://pubs.rsc.org/en/content/articlelanding/2010/ee/c0ee00092b > .

[28] Giglio E, Lanzini A, Santarelli M, Leone P. Synthetic natural gas via integrated high-temperature electrolysis and methanation: Part II—Economic analysis. J Energy Storage 2015;2:64–79. https://doi.org/10.1016/j.est.2015.06.004. < http://www.sciencedirect.com/science/article/pii/S2352152X15300013 > .

[29] Giglio E, Lanzini A, Santarelli M, Leone P. Synthetic natural gas via integrated high-temperature electrolysis and methanation: Part I—Energy performance. J Energy Storage 2015;1:22–37. https://doi.org/10.1016/j.est.2015.04.002. < http://www.sciencedirect.com/science/article/pii/S2352152X15000067 > .

[30] Buttler A, Koltun R, Wolf R, Spliethoff H. A detailed techno-economic analysis of heat integration in high temperature electrolysis for efficient hydrogen production. Int J Hydrogen Energy 2015;40(1):38–50. https://doi.org/10.1016/j.ijhydene.2014.10.048. < http://www.sciencedirect.com/science/article/pii/S0360319914028511 > .

[31] Reytier M, Di Iorio S, Chatroux A, Petitjean M, Cren J, De Saint Jean M, et al. Stack performances in high temperature steam electrolysis and co-electrolysis. Int J Hydrogen Energy 2015;40(35):11370–7. https://doi.org/10.1016/j.ijhydene.2015.04.085.

[32] Reiter G, Lindorfer J. Evaluating CO2 sources for power-to-gas applications: a case study for Austria. J CO2 Util 2015;10:40–9. https://doi.org/10.1016/j.jcou.2015.03.003.

[33] Cheng J. Biomass to renewable energy processes. CRC Press; 2017.

[34] Blanco H, Nijs W, Ruf J, Faaij A. Potential of power-to-methane in the EU energy transition to a low carbon system using cost optimization. Appl Energy 2018;232:323–40. https://doi.org/10.1016/j.apenergy.2018.08.027. < http://www.sciencedirect.com/science/article/pii/S0306261918311826 > .

[35] Köppel W, Götz M, Graf F. Biogas upgrading for injection into the gas grid. Gwf-Gas Erdgas 2009;150:26–35.

[36] Vo TTQ, Wall DM, Ring D, Rajendran K, Murphy JD. Techno-economic analysis of biogas upgrading via amine scrubber, carbon capture and ex-situ methanation. Appl Energy 2018;212:1191–202. https://doi.org/10.1016/j.apenergy.2017.12.099. < http://www.sciencedirect.com/science/article/pii/S0306261917318226 > .

[37] Witte J, Calbry-Muzyka A, Wieseler T, Hottinger P, Biollaz SMA, Schildhauer TJ. Demonstrating direct methanation of real biogas in a fluidised bed reactor. Appl Energy 2019;240:359–71. https://doi.org/10.1016/j.apenergy.2019.01.230. < http://www.sciencedirect.com/science/article/pii/S0306261919302594 > .

[38] Dumont E. H2s removal from biogas using bioreactors: a review. Int J Energy Environ 2015;6(5):479–98 < https://hal.archives-ouvertes.fr/hal-01945143 > .

[39] Krayzelova L, Bartacek J, Díaz I, Jeison D, Volcke EI, Jenicek P. Microaeration for hydrogen sulfide removal during anaerobic treatment: a review. Rev Environ Sci Bio/Technol 2015;14(4):703–25. https://doi.org/10.1007/s11157-015-9386-2.

[40] Díaz I, Ramos I, Fdz-Polanco M. Economic analysis of microaerobic removal of h2s from biogas in full-scale sludge digesters. Bioresource Technol 2015;192:280–6.

[41] Hansen JB, Fock F, Lindboe HH. Biogas upgrading: by steam electrolysis or co-electrolysis of biogas and steam. ECS Trans 2013;57(1):3089–97.

[42] Lorenzi G, Lanzini A, Santarelli M, Martin A. Exergo-economic analysis of a direct biogas upgrading process to synthetic natural gas via integrated high-temperature electrolysis and methanation. Energy 2017;141:1524–37. https://doi.org/10.1016/j.energy.2017.11.080. < http://www.sciencedirect.com/science/article/pii/S0360544217319382 > .

[43] Chen XY, Vinh-Thang H, Ramirez AA, Rodrigue D, Kaliaguine S. Membrane gas separation technologies for biogas upgrading. Rsc Adv 2015;5(31):24399–448.

[44] Basu S, Khan AL, Cano-Odena A, Liu C, Vankelecom IF. Membrane-based technologies for biogas separations. Chem Soc Rev 2010;39(2):750–68.

[45] Turton R, Bailie RC, Whiting WB, Shaeiwitz JA. Analysis, synthesis and design of chemical processes. Pearson Education. google-Books-ID: kWXyhVXztZ8C; 2008.

[46] Wang L, Yang Z, Sharma S, Mian A, Lin T-E, Tsatsaronis G, et al. A review of evaluation, optimization and synthesis of energy systems: methodology and application to thermal power plants. Energies 2019;12(1):73.